

## ON-LINE APPENDIX: SUPPLEMENTARY METHODS

### Elimination of Side-Branching Vessels

Ophthalmic arteries were eliminated in each model. The posterior communicating artery (PcomA) is included in model 1, but the remaining models are truncated just proximal to its origin. To determine the effects of side-branching vessels on intra-aneurysmal hemodynamics, we performed pretreatment CFD simulations of the fourth patient including the ophthalmic artery and assumed Murray law scaling (the ratio of the flow rates is equal to the cube ratio of the diameters, keeping WSS constant) for the ophthalmic flow rate. The flow in the ophthalmic artery was 1.2% of the ICA flow, which affected the shear stress and pressure drop in the aneurysm dome by much less than 1%. Because the diameter of the ophthalmic artery was similar in the other 3 models, we assumed a negligible influence, considering that errors in segmentation are approximately 10%. Thus, these and other smaller side-branching vessels were not included in CFD simulations. However, because of the proximity of the aneurysm in patient 1 to the large PcomA, we included it in the analysis after Murray law calculations determined a flow ratio of 7.26 between PcomA and terminal ICA.

### Equations for Shear Stress and Shear Stress Gradient

We denoted the wall shear stress vector at position  $\mathbf{x}$  and time  $t$  as  $\vec{\tau}(\mathbf{x}, t)$ , which is composed of 2 independent components:  $\tau_s$ , the vector acting along the axis of the vessel, and  $\tau_m$ , acting in a plane parallel to the vessel wall. The shear stress vector is related to the instantaneous wall shear stress magnitude,  $\tau(\mathbf{x}, t)$ , by the expression

$$\tau(\mathbf{x}, t) \equiv |\vec{\tau}(\mathbf{x}, t)| = (\tau_s^2(\mathbf{x}, t) + \tau_m^2(\mathbf{x}, t))^{1/2}$$

where  $|\cdot|$  denotes the absolute value of a vector. We computed the time-averaged wall shear stress, TAWSS( $\mathbf{x}$ ), over  $n$  number of cardiac cycles by use of the expression

$$\text{TAWSS}(\mathbf{x}) = \left| \frac{1}{n \cdot T} \int_0^{n \cdot T} \vec{\tau}(\mathbf{x}, t) dt \right|$$

where  $T$  is the period of the cardiac cycle. Similarly, we defined the wall shear stress gradient magnitude, denoted WSSG( $\mathbf{x}, t$ ), by

$$\text{WSSG}(\mathbf{x}, t) \equiv \left( \left( \frac{\partial \tau_s}{\partial s} \right)^2 + \left( \frac{\partial \tau_m}{\partial m} \right)^2 \right)^{1/2}.$$

Last, we calculated the time-averaged wall shear stress gradient, TAWSSG( $\mathbf{x}$ ), by integrating over  $n$  number of cardiac cycles with the expression

$$\text{TAWSSG}(\mathbf{x}) = \frac{1}{n \cdot T} \int_0^{n \cdot T} \text{WSSG}(\mathbf{x}, t) dt.$$

### Treatment of the Stent as a Porous Surface

In our simulations, we treated the flow-diverting stent as a thin, porous surface, meaning that one treats the net effect of the stent as a sink of momentum to the flowing blood. The advantage of this approach is that one does not have to fully resolve the flow around individual stent struts, but one still captures the bulk effect of the stent on the flow. The momentum sink of the stent is proportional to the fluid velocity across the stent. We assumed that the stent is a homogeneous porous surface so that the sink for the fluid momentum equation is written as

$$S_i = - \left( \frac{\mu}{\alpha} u_i + \frac{1}{2} C \rho |u| u_i \right)$$

where the  $i$  subscript is the  $i$ th vector component,  $u$  is the fluid velocity,  $\rho$  is the fluid density,  $\mu$  is the fluid viscosity, and  $\alpha$  and  $C$  are the loss coefficients of the stent's porous surface. In all simulations, we used values of  $\alpha = 7.1 \cdot 10^{-10} \text{ m}^2$  and  $C = 1.4 \cdot 10^{-4} \text{ m}^{-1}$ , which are derived from the incorporation of stent porosity and strut thickness values into previous methods of CFD modeling of flow-diverting stents.<sup>1</sup> This method does not take into account the effects of stent deformation on porosity, a limitation of the present methods.<sup>2</sup>

## REFERENCES

1. Augsburger L, Reymond P, Rufenacht DA, et al. Intracranial stents being modeled as a porous medium: flow simulation in stented cerebral aneurysms. *Ann Biomed Eng* 2011;39:850–63
2. Mut F, Cebal JR. Effects of flow-diverting device oversizing on hemodynamics alteration in cerebral aneurysms. *AJNR Am J Neuroradiol* 2012;33:2010–16

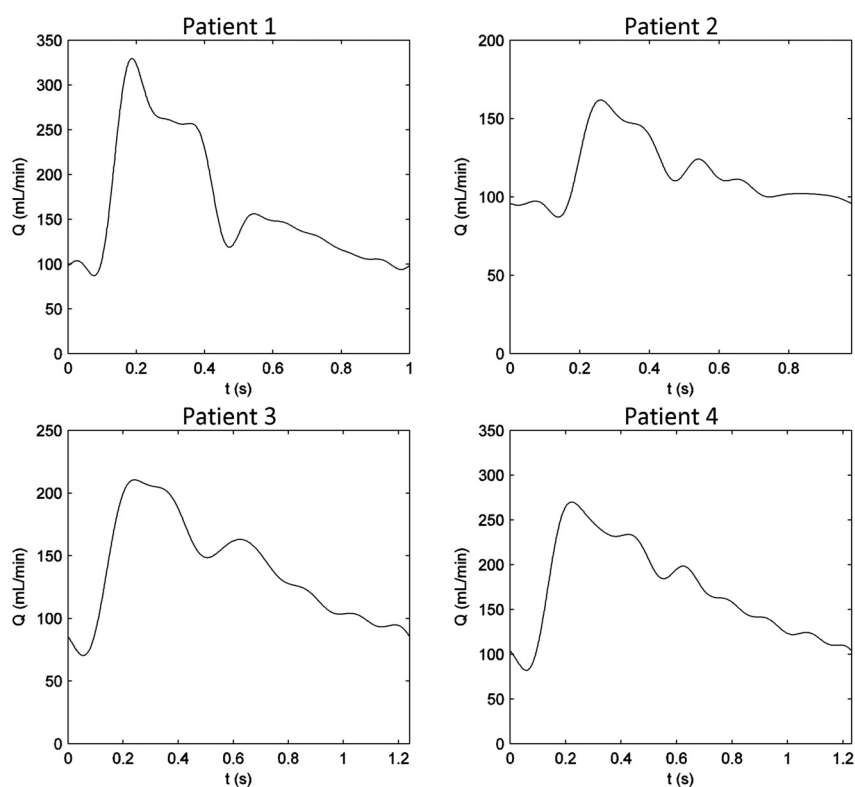
**On-line Table 1: Patient and aneurysm characteristics**

<i>n</i>	Age, y	Sex	Aneurysm Location	Neck Width, mm	Aneurysm Volume, cm <sup>3</sup>	Parent Artery Diameter, mm	Stent Diameter and Length, mm
1 <sup>a</sup>	75	Male	Left supraclinoid internal carotid	10.6	3.8	4.29	4.5 × 25
2	64	Female	Left supraclinoid internal carotid	3.6	0.21	3.48	4 × 20
3	77	Female	Left paraclinoid internal carotid	4.9	1.31	3.85	4 × 16
4	46	Female	Left carotid cave	5	0.02	4.41	4.25 × 16

<sup>a</sup>Patient treated with both flow-diverting stent and coils.

**On-line Table 2: Pressure drops (in mm Hg) simulated with the use of computational modeling before and after aneurysm treatment**

<i>n</i>	Averaged Over Cardiac Cycle		Peak Systolic Values	
	Pretreatment	Posttreatment	Pretreatment	Posttreatment
1	2.89	2.58	8.72	4.83
2	1.85	1.53	3.30	2.77
3	1.00	1.12	2.03	2.60
4	1.14	1.30	2.47	2.90
Average	1.72	1.63	4.13	3.27
Standard deviation	0.86	0.65	3.11	1.04
<i>P</i>		.55		.47



**ON-LINE FIG 1.** Averaged waveforms of blood flow during a single cardiac cycle for each patient as incorporated into pretreatment inflow conditions.